Mechanical Properties of the Flexible-Type Epoxy/Clay Nanocomposites Prepared by Slurry Method

Miyuki Harada, Ayumu Ueda, Hironori Miyazaki, Mitsukazu Ochi

Department of Chemistry and Materials Engineering, Faculty of Chemistry, Materials and Bioengineering, Kansai University, Suita-shi, Osaka 564-8680, Japan

Received 7 October 2008; accepted 25 January 2009
DOI 10.1002/app.30396
Published online 27 April 2009 in Wiley InterScience (www.interscience.wiley.com).

ABSTRACT: The bisphenol-F type flexible epoxy resin, having a good flexibility, was combined with an organo- and slurry-clay. The clay dispersions in the obtained epoxy/clay systems are significantly different depending on the type of clay. Particularly, the epoxy/slurry-clay system showed a high clay dispersibility into the epoxy matrix and was transparent in spite of the addition of 10 wt % clay. This result means that the swelling of the clay with formamide is effective for the expansion of the basal spacing of the clay. The slurry-clay nanocomposite (clay content: 5 wt %) showed a 4 times higher fracture energy than the neat epoxy system in the tensile test, though the organo-clay system (clay content: 5 wt %) was 1.5 times higher. © 2009 Wiley Periodicals, Inc. J Appl Polym Sci 113: 2256–2263, 2009

Key words: clay; dispersions; nanocomposites; toughness

INTRODUCTION

Recently, polymer/clay nanocomposite, which are a kind of organic–inorganic nanocomposite, have been extensively studied, because of their high modulus,[1,2] gas barrier property,[3,4] and low water absorption property[5] by dispersion of a small amount of nanoscale layered filler having a high aspect ratio into the polymer matrix. Most research studies have involved clay nanocomposites based on thermoplastic polymers. Usuki et al.[6–8] reported that ω-amino acid intercalated into clay was polymerized at the clay interlayer and formed a well-dispersed clay nanocomposite.

However, in clay nanocomposites based on thermosetting polymers, though the nanocomposites based on a high T_g polymer matrix show a relatively high modulus and fracture toughness,[9,10] their deformability decreased more than that of neat resins[11] in most cases. However, most of the nanocomposites based on a rubbery polymer matrix showed an improvement in their deformability and fracture energy with the addition of clays. Lan and Pinnavaia[12] reported that when the rubbery matrix is used, an epoxy/clay nanocomposite shows a high mechanical property. Boukerrou et al.[13] reported that the epoxy/clay system cured with a polyoxypropylene-type diamine shows not only a high modulus, but also a deformation greater than the neat epoxy and clay nanocomposite. Similarly, Wang et al.[14] also reported that the low T_g polyurethane-based clay nanocomposite showed an increase in the crack-spreading path during tensile drawing. These results mean that the increase in the crack-spreading path around the clay layers can produce a higher energy consumption.

However, to obtain well-dispersed polymer/clay nanocomposites, two techniques, that is, direct mixing[9] and solution mixing[5–15] are well known. The latter technique is very effective for the uniform dispersion of a clay into the matrix. In most cases, polar solvents are selected, such as acetone, DMF, and DMAc. Yang et al.[2] prepared the PU/clay nanocomposite utilizing an organo-clay treated by 12-aminododecanoic acid using the DMF swelling method. This system showed a high degree of exfoliation and its thermal and mechanical properties were significantly improved with the increasing clay content.

In this study, two types of clays (organo-clay and slurry-clay utilizing a polar solvent) were prepared. The epoxy and curing agent to obtain a rubbery matrix was selected and the epoxy/clay nanocomposites with a flexible matrix were prepared. The relationship between the clay dispersibility and mechanical properties of the nanocomposites was investigated in detail.

EXPERIMENTAL

Materials

The epoxy resin used in this study was the diglycidyl ether of the bisphenol F-type flexible epoxy resin (YL7175-1000, JER Co., Epoxy equivalent = 1159 g/equiv),

Correspondence to: M. Harada (mharada@ipcku.kansai-u.ac.jp).

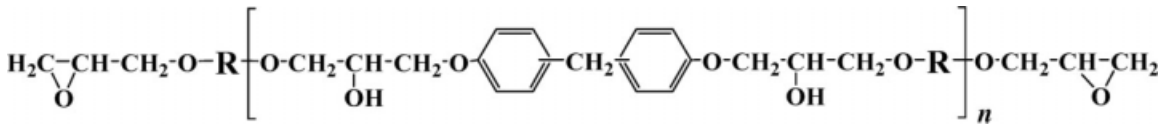

The curing agent was polyoxypropylamine (Jeffamine-D230, Santechno Chemical Co., Amine equivalent = 57.5 g/equiv).

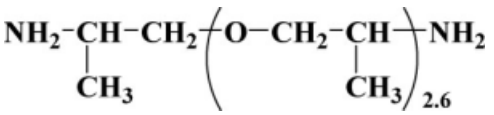

As a filler, a layered clay (Nanomer I.22E, a cation exchange capacity of 80∼120 mequiv/100 g, Bolclay Japan Co.) was used. The organo-clay was obtained by treatment with octadecylamine (Wako Chemical Co., $M_w = 269$).

Preparation of the organo-clay

An untreated clay (7.0 g) was dispersed into a flask of distilled water (560 mL) at 80°C for 2 h. In another flask, distilled water (172 mL), 35% HCl (1 mL), and octadecylamine (3.25 g, this quantity corresponds to 1.5 equivalents for the cation exchange capacity) were mixed to make an octadecyl ammonium salt at 80°C for 1 h. The dispersed clay was then mixed with the aqueous solution of the ammonium salt and stirred at 80°C for 2 h to make cation exchange. After the filtration, the organo-modified clay was washed by the mixed solvent (ethanol/distilled water = 1 : 1(w/w)) at 60°C. This process was done to remove any residue of the ammonium salt of octadecylamine. The complete removal of the chloride ions was confirmed by the addition of $AgNO_3$. The organo-clay was dried in a vacuum oven at 75°C for 20 h, and then ground for 1 min.

Preparation of the epoxy/oragano-clay nanocomposite

A mixture of the organo-clay and epoxy resin was stirred at 120°C and 250 rpm for 10 h and then degassed at 70°C for 6 h under reduced pressure. After adding a stoichiometric amount of the curing agent, the mixture was cured at 80°C for 20 min under reduced pressure. It was then cured at 80°C for 100 min, 150°C for 4 h, and 180°C for 1 h under normal pressure. It was confirmed by FTIR measurements that the final conversion of the epoxy groups in the cured resin was over 90%.

Preparation of the slurry-clay

Untreated clay (3.0 g) was added to formamide (9.0 g) (Wako Chemical Co., b.p.: 210°C) as the swelling solvent. The mixture was stirred at r.t. and 100 rpm for 3 h.

Preparation of the epoxy/slurry-clay nanocomposite

A mixture of the slurry-clay and epoxy resin was stirred at 70°C and 250 rpm, for 10 h and distilled water at 70°C was added to exchange the formamide as the solvent having the lower boiling point. It was then degassed at 70°C for 6 h under reduced pressure. After adding a stoichiometric amount of the curing agent, the mixture was cured at 80°C for 20 min under reduced pressure. It was then cured at 80°C for 100 min, 150°C for 4 h, and 180°C for 1 h in normal pressure. It was confirmed by FTIR measurements that the final conversion of the epoxy groups in the cured resin was over 90%.

Measurements

The chemical conversion of the epoxy groups was confirmed by FTIR spectroscopy (SPECTRUM 2000, Perkin-Elmer Co.). The KBr tablet method was used. X-ray diffraction (XRD, R-AXIS, Rigaku Co.) was used to evaluate the basal spacing of the layered clay. The basal spacing was calculated by the Bragg's formula ($n\lambda = 2d \sin\theta$). Diffraction patterns were obtained using Cu Kα ($\lambda = 0.154$ nm) radiation generated at 40 kV and 60 mA. The untreated and organo-clay powder and slurry-clay paste containing untreated clay and formamide were placed on a sample holder and a smooth surface was obtained by pressing and scraping the clay. The nanocomposites were cut out by the size of 5.0 × 15.0 × 1.5 mm^3.

Optical photographs were obtained using an digital camera (FE-180,Olympus). The sample dimensions were 20.0 × 30.0 × 4.0 mm^3. The surfaces of the nanocomposites were not polished.

The morphologies of the clays and the composites were observed using a scanning electron microscope (SEM, JSM-6700F, JEOL Co.). The samples were obtained by cutting of the nanocomposites in liquid N_2.Before the examination, the surfaces were coated with a thin amorphous osmium layer (about 5 nm) (MEIWA FOSIS Co.) to improve the conductivity and prevent charging.

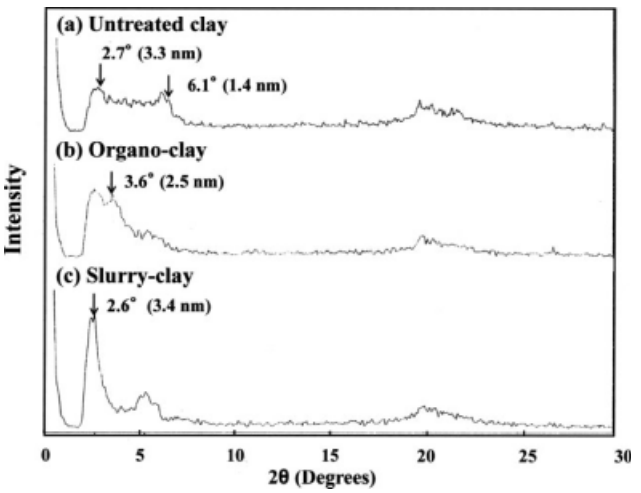

Figure 1 X-ray diffraction of the (a) untreated, (b) organo-, and (c) slurry-clays.

The morphology of the composites was also observed using a transmission electron microscope (TEM, JEM-1210, JEOL Co.). An ultra-thin section of the specimen for the TEM observations was prepared using an ultramicrotome (Reichert Ultracut E, Leica Co.) with a diamond knife. The specimens were not treated with any staining techniques. The thickness of the specimens was 50 nm and the acceleration voltage was 120 kV.

A dynamic mechanical analysis of the cured system was completed using a nonresonance forced vibration viscoelastometer (DVE-V4, Rheology Co.) in the tension mode. The frequency and amplitude of the vibration were adjusted to 10 Hz and ±5 μm, respectively. The heating rate was 2°C/min and the measured temperature range was from –150 to 250°C. The sample dimensions were approximately $4.0 \times 30.0 \times 0.3$ mm^3.

The tensile property was measured according to JIS K-7113. The specimen was formed by a mold tool (No. 6, Taiyu kizai Co.) and the length was 75.0 mm. The width and thickness of the specimen was 4 mm and 2 mm, respectively. It was mounted in an Instron-type tensile machine (AGS-J, Shimazu Co.) and loaded at a constant crosshead speed (2.0 mm/min). The fracture energy of cured systems in tensile test was calculated from the area under the stress–strain curves.

The pencil hardness was measured according to JIS-5600-5-4. The thickness of the specimen was 500 μm. Pencils with a hardness from 6B to 9H (HI-Uni, Mitsubishi Co.) were used.

RESULTS AND DISCUSSION

Evaluation of the basal spacing of organo-clay and slurry-clay

The XRD peaks of the neat, organo-, and slurry-clays are shown in Figure 1. The untreated clay showed a broad peak between 2.6° and 6.1° in 2θ. This means that the clay basal spacing is not composed of a single distance. As the used clay is a natural product, the distribution of the clay's quality affects their

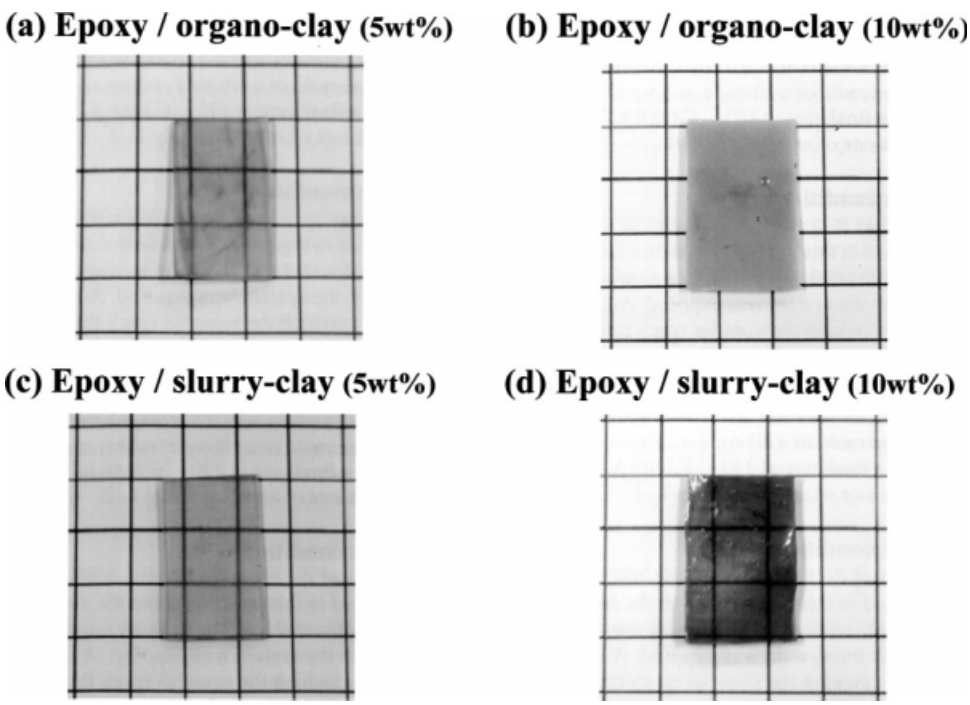

Figure 2 Optical micrographs of the epoxy/clay nanocomposites.

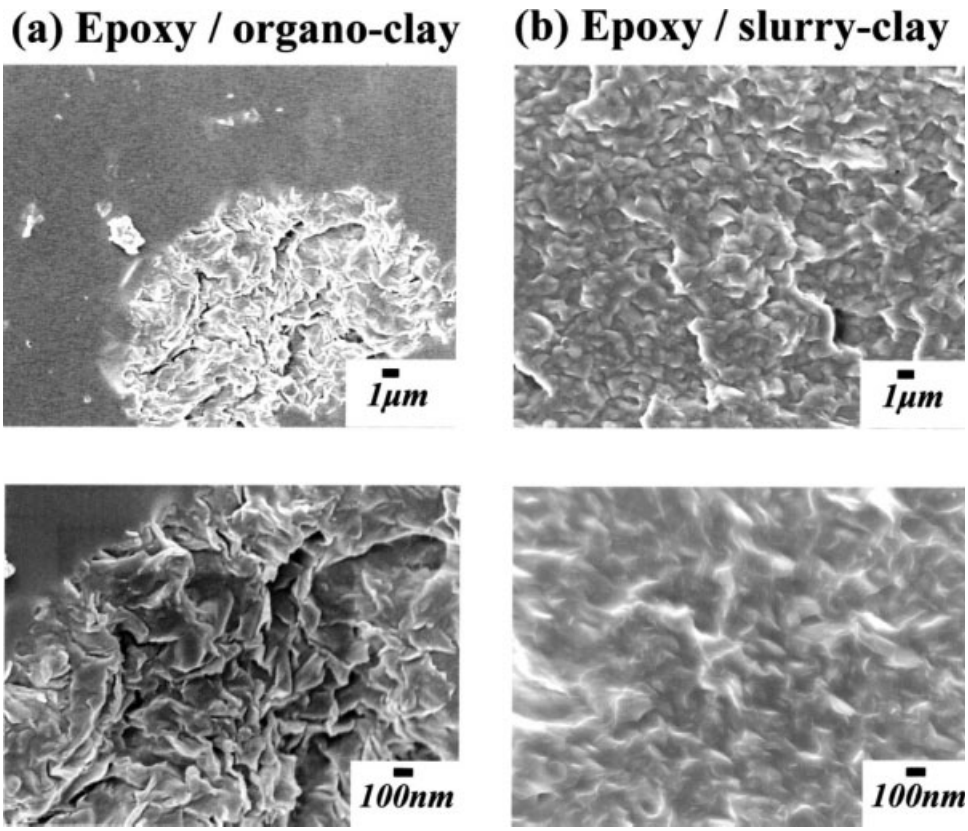

Figure 3 SEM photographs of the epoxy/clay nanocomposites (clay content: 5 wt %).

basal spacing. This result indicates that the unmodified clays have various basal spacings between 1.4 and 3.3 nm. On the other hand, the organo-clay, which was obtained by the octadecylamine treatment of an unmodified clay, showed higher intensity peaks at a low angle (2.7 degrees) compared to the unmodified clay. At the same time, the higher angle peak of 2θ shifted to a narrow degree. This means

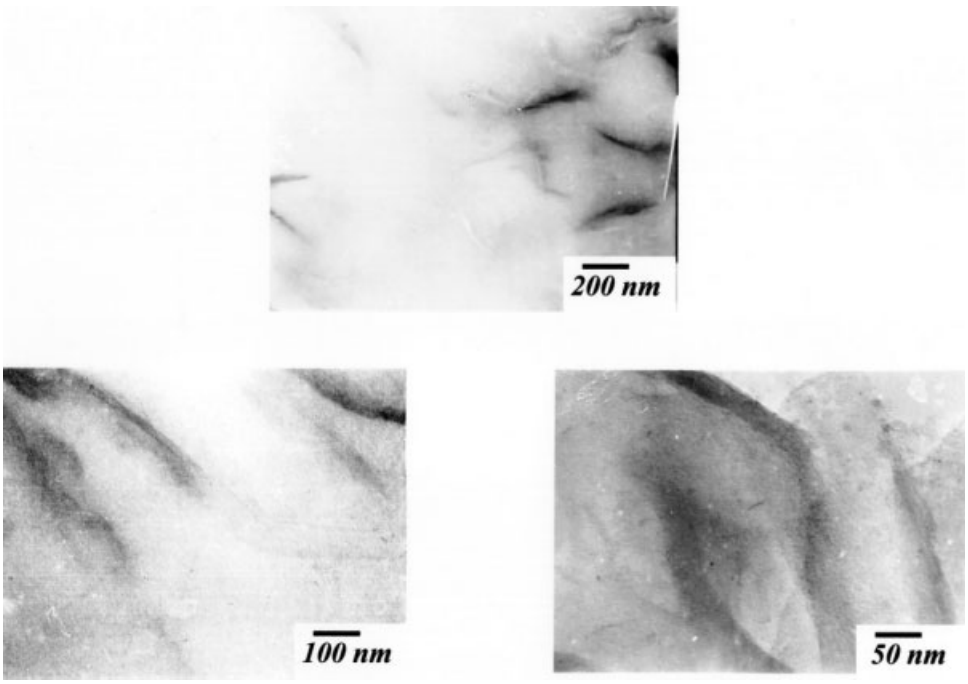

Figure 4 TEM photographs of the epoxy/slurry-clay nanocomposites (clay content: 5 wt %).

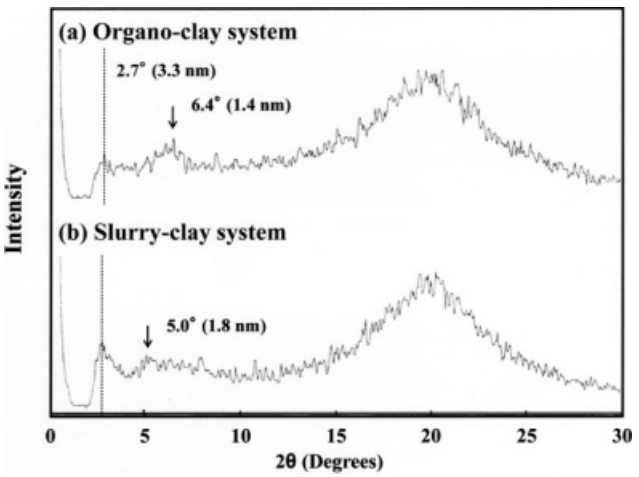

Figure 5 X-ray diffraction of the epoxy/slurry-clay nanocomposites (clay content: 5 wt %).

that the basal spacing of the organo-clay becomes quite uniformly higher due to intercalation of the octadecylamine. Moreover, the slurry-clay showed sharp peaks at the lower angles. These results mean that the interlayer of the slurry clay expands more than that of the other clays and the basal spacing of the clay is greater than 3 nm. However, it could not be observed the other peaks at the lower angle. This is due to the minimum limit of detection in XRD.

Dispersibility of the clay in epoxy/clay nanocomposites

The transparency of the obtained composites was investigated. Figure 2 shows the external appearance of the organo- and slurry- clay systems (clay contents: 5 and 10 wt % systems). In the 5 wt % system, both clay-modified systems showed a relatively high transparency, regardless of the 2 mm sample thickness. However, with an increase in the clay content, the transparency only in the organo-clay nanocomposite dramatically decreased and became opaque in the 10 wt % clay system. This result is derived from the poor dispersion of the layered clay in the organo-clay system, and it is considered that the slurry-clay nanocomposite should attain a high clay dispersion.

The detail morphologies of the organo- and slurry-clay systems were examined using an SEM. Figure 3 shows the fracture surface of each systems. In the (a) organo-clay system, a large aggregated region of layered clays and no-clay dispersed region were observed. Although the organo-clay (5 wt %) composite showed transparency in the previous visual observation, it is found that the system contained a lot of clay aggregations. Because the concentration of the clay aggregations naturally increases at the high clay content, this may be related to the sample opacity in the 10 wt % system. On the other hand, (b) the slurry-clay systems showed a relatively uniform clay dispersion. Moreover, the non-clay dispersed regions were not found in a high magnification photograph of this system. From this result, it can be also confirmed that the slurry method system has a better dispersion.

The TEMs of the slurry method system (Clay content: 5 wt %) are shown in Figure 4. Although the layered clays showed a good dispersion in the photographs at all magnifications, the composite contains some stacked clays. These photographs mean that the clay disperses as several stacked layers into the matrix. In the XRD spectra (Fig. 5), (b) the slurry-clay composite showed diffraction peaks at

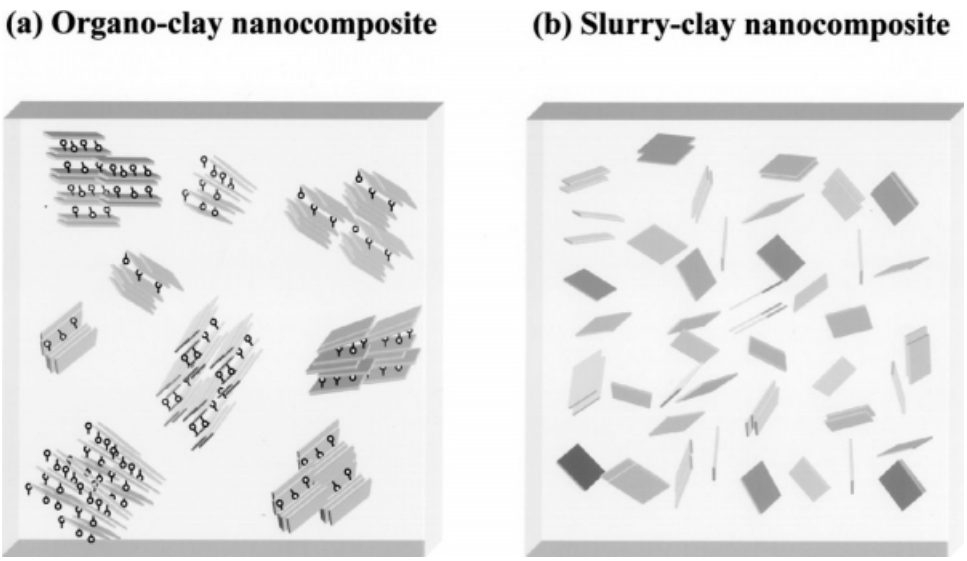

Figure 6 Clay dispersion in the epoxy/clay nanocomposites.

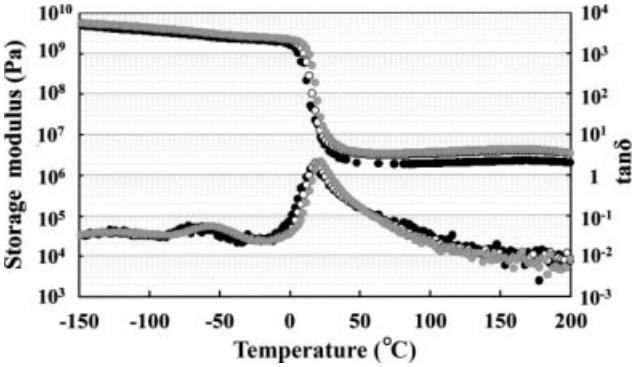

Figure 7 Dynamic mechanical analysis of the (●) neat epoxy, (○) epoxy/organo-clay, and (●) slurry-clay nanocomposites (clay content: 5 wt %).

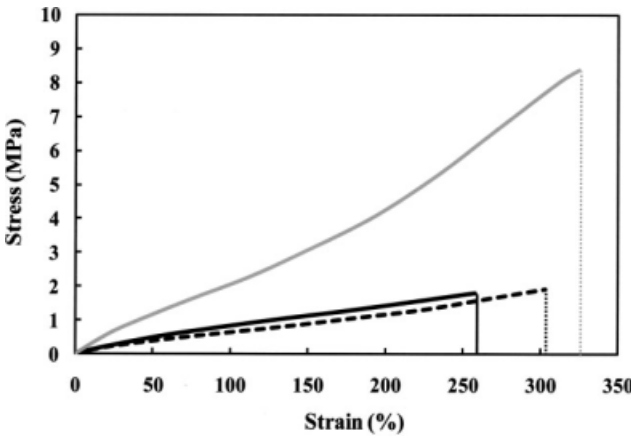

Figure 8 Stress–strain curves of the (—) neat epoxy, (---) epoxy/organo-clay, and (—) slurry-clay nanocomposites (clay content: 5 wt %).

2.7, 5.0, 20 degrees. The peak at 20 degrees showed an amorphous halo derived from the epoxy network structure. The other peaks showed the basal spacing of the layered clays and their values are 1.8–3.3 nm. However, it could not be observed the other peaks at the lower angle as mentioned above. This is due to the minimum limit of detection in XRD. Based on these results, the models of the clay composites are shown in Figure 6. The organo-clay nanocomposite has a large scale aggregation of clays in the matrix and the basal spacing of almost all the clays is 1.4 nm. On the other hand, the slurry clay nanocomposite has a good dispersion of the clays, though they are composed of several stacked structures.

Thermomechanical property of the epoxy/clay nanocomposites

The temperature dependence of the dynamic mechanical properties of the neat epoxy systems and organo- and slurry-clay nanocomposites are shown in Figure 7 and Table I. The storage modulus of all the systems showed a significant decrease at 20°C. This phenomenon is due to the glass-rubbery transition around 20°C and showed that this epoxy resin (Bisphenol-F type, flexible epoxy resin) has a relatively low T_g for containing the flexible long chains. At the same time, the tan δ at 20°C of all the systems showed significantly broad peaks. It is considered to be due to the distribution of the molecular weight of the used epoxy monomer and curing agent, because the curing temperature is sufficiently higher than the T_g of this system. Although the T_g of the neat epoxy was 16°C, the clay nanocomposites showed slightly higher temperatures of 18°C (in organo-clay nanocomposite) and 22°C (in the slurry-clay composite). This result means that the glass transition temperature increases with the improvement in the clay dispersion. It is considered that this phenomenon is due to the addition of the layered clay as an inorganic component having a high heat resistance and the suppression of molecular motion around the dispersed clays. Moreover, the storage modulus of the neat epoxy in the rubbery plateau region over 50°C was 1.9 MPa. In the organo- and slurry-clay nanocomposites, the storage modulus in the rubbery region was about 2 times higher than that of the neat epoxy system in the same high temperature region even for the 5 wt % clay content.

To evaluate their mechanical properties, the stress–strain curves were obtained from the tensile test (Fig. 8). The neat epoxy system showed a considerably small ultimate stress, but a large ultimate

TABLE I
T_g and Storage Modulus of the Epoxy/Clay Nanocomposites

Curing system	T_g (°C)	Storage modulus at −50°C (Pa)	Storage modulus at 100°C (Pa)
Neat epoxy resin	16	2.50×10^9	1.9×10^6
Epoxy/organo-clay (5 wt %)	18	2.98×10^9	3.3×10^6
Epoxy/slurry-clay (5 wt %)	22	3.07×10^9	3.6×10^6

TABLE II
The Tensile Properties of the Epoxy/Clay Nanocomposites

Curing system	Ultimate stress (MPa)	Ultimate strain (%)	Fracture energy (kJ/m^2)
Neat epoxy resin	1.8 ± 0.1	257.8 ± 12.9	72.2 ± 6.9
Epoxy/organo-clay (5 wt %)	1.9 ± 0.1	303.4 ± 13.7	104.6 ± 10.1
Epoxy/slurry-clay (5 wt %)	8.4 ± 0.2	324.5 ± 7.8	293.2 ± 14.3

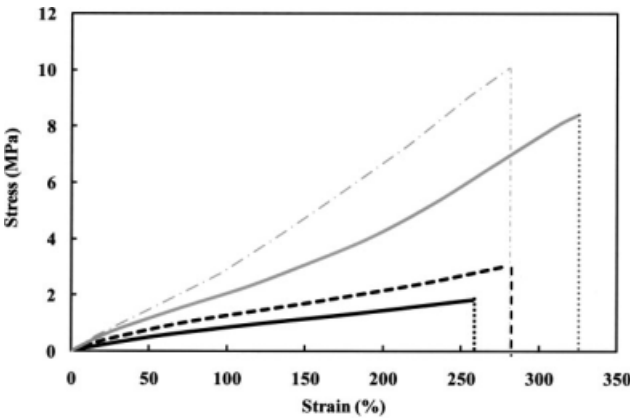

Figure 9 Stress–strain curves of the (—) neat epoxy and slurry-clay nanocomposites. Clay content: (---) 1 wt %, (—) 5 wt %, and (- - - - -) 10 wt %.

strain. Although the organo-clay nanocomposite showed almost the same stress compared to the neat resin system, the ultimate strain was slightly improved. However, the slurry-clay systems had significantly improved not only the ultimate strain, but also the ultimate stress. As the results, the fracture energy of the slurry nanocomposite was 4 times higher than the neat resin (Table II).

The clay content dependence of the tensile property was then investigated. The stress–strain curves of the 0–10 wt % clay content systems are shown in Figure 9. The modulus, which is estimated from the incline of the curves, increased with an increase in the clay content. On the other hand, the ultimate strain of these systems showed a maximum value at the 5 wt % clay content and decreased at the 10 wt % clay content. It is predicted that the collision of clays would occur when the specimens are extensively deformed by the loading of the tensile stress. The stress concentration at the interfaces between the matrix resin and dispersed clays causes a decrease in the strain. Actually, the stress–strain curves are nonlinearly drawn and the enhanced incline of the curves means an inducement of the clay collision derived from the large scale deformation of the matrix. As shown in Figure 10, it is supposed that the increase in the fracture energy by adding clay will saturate between from 5 to 10 wt % clay content, because the ultimate stress and strain shows trade-off relationship. This result is derived from the hardening of the composite with the excess addition of the high modulus filler (Table III).

TABLE III
The Tensile Properties of the Epoxy/Clay Nanocomposites Having Different Clay Content

Curing system	Ultimate stress (MPa)	Ultimate strain (%)	Fracture energy (kJ/m^2)
Neat epoxy resin	1.8 ± 0.1	257.8 ± 12.9	72.2 ± 6.9
Epoxy/slurry-clay (1 wt %)	3.0 ± 0.1	280.3 ± 6.9	117.0 ± 7.1
Epoxy/slurry-clay (5 wt %)	8.4 ± 0.2	324.5 ± 7.8	293.2 ± 14.3
Epoxy/slurry-clay (10 wt %)	10.1 ± 0.3	281.0 ± 9.1	309.7 ± 22.7

The pencil hardness of the composites is shown in Figure 11. The pencil hardness increased with the addition of the clay as an inorganic component the same as the case of the tensile modulus. For the pencil hardness, it showed a maximum value at the 5 wt % clay content and retained this value up to 10 wt %. These results suggest that the increase in the well-dispersed clays determined the hardness of the composites.

CONCLUSIONS

The bisphenol-F type, flexible epoxy resin/slurry-clay composite showed a highly clay dispersion in

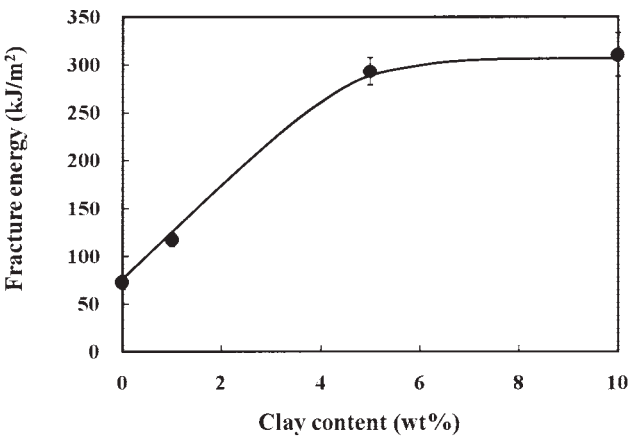

Figure 10 Fracture energy of the neat epoxy and slurry clay nanocomposites.

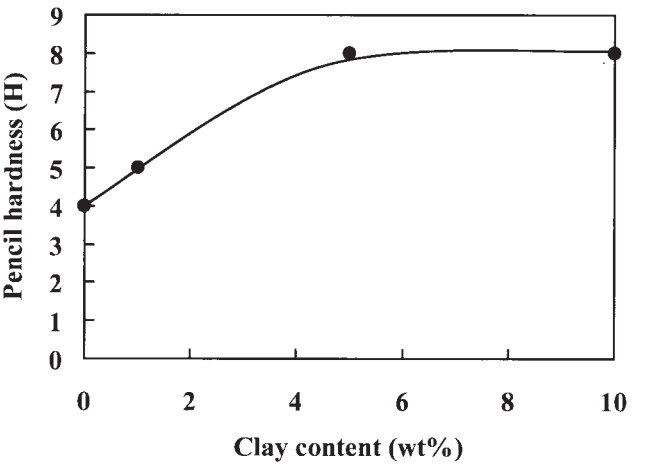

Figure 11 Pencil hardness of the neat epoxy and slurry clay nanocomposites.

the epoxy matrix and also showed a transparency in spite of the addition of 10 wt % clays. This means that the swelling of the untreated clay using a polar solvent is effective for the expansion of the basal spacing of the clay. The slurry-clay nanocomposite (clay content: 5 wt %) showed a 4 times higher fracture energy than the neat epoxy system and the hardness was also improved.

References

1. Boo, W. J.; Sun, L.; Warren, G. L.; Moghbelli, E.; Pham, H.; Clearfield, A.; Sue, H. J. Polymer 2007, 48, 1075.
2. Cshen-Yang, Y. W.; Lee, Y. K.; Chen, Y. T.; Wu, J. C. Polymer 2007, 48, 2969.
3. Ogasawara, T.; Ishida, Y.; Ishikawa, T.; Aoki, T.; Ogura, T. Compos A 2006, 37, 2236.
4. Yano, K.; Usuki, A.; Okada, A.; Kurauchi, T.; Kamigaito, O. J Polym Sci Part B: Polym Phys 1993, 31, 2493.
5. Liu, W.; Hoa, S.; Pugh, M. Compos Sci Mater 2005, 65, 2364.
6. Usuki, A.; Kawasumi, M.; Kojima, Y.; Okada, A.; Karauchi, T. J Mater Res 1993, 8, 1174.
7. Usuki, A.; Kojima, Y.; Kawasumi, M.; Okada, A.; Fukushima, Y. J Mater Res 1993, 8, 1179.
8. Usuki, A.; Tsukigase, A.; Kato, M. J Appl Polym Sci 2004, 93, 758.
9. Liu, T.; Tjiu, W.; Tong, Y.; He, C.; Goh, S.; Chung, T. J Appl Polym Sci 2004, 94, 1236.
10. Liu, W.; Hoa, S.; Pugh, M. Compos Sci Technol 2005, 65, 307.
11. Nigam, V.; Setua, D.; Mathur, G.; Kar, K. J Appl Polym Sci 2004, 93, 2201.
12. Lan, T.; Pinnavaia, T. Chem Mater 1994, 6, 2216.
13. Boukerrou, A.; Duchet, J.; Fellahi, S.; Kaci, M.; Sautereau, H. J Appl Polym Sci 2007, 103, 3547.
14. Wang, J.; Chen, Y.; Chen, R. J Polym Sci Part B: Polym Phys 2007, 45, 519.
15. Wang, K.; Chen, L.; Wu, J.; Toh, M.; He, C.; Yee, A. Macromolecules 2005, 38, 788.